ISSN 1990-3413, Astrophysical Bulletin, 2016, Vol. 71, No. 3, pp. 257–269. © Pleiades Publishing, Ltd., 2016.
Original Russian Text © F.G. Kopylova, A.I. Kopylov, 2016, published in Astrofizicheskii Byulleten', 2016, Vol. 71, No. 3, pp. 279–292.

The Fundamental Plane and Other Scaling Relations for Galaxy Groups and Clusters

F. G. Kopylova* **and A. I. Kopylov**

Special Astrophysical Observatory, Russian Academy of Sciences, Nizhnii Arkhyz, 369167 Russia

Received January 14, 2016; in final form, June 13, 2016

Abstract—In this paper we study the relations between the main characteristics of groups and clusters of galaxies using the archival data of the SDSS and 2MASX catalogs. We have developed and implemented a new method of determining the size of galaxy systems and their effective radius which contains half of the galaxies and not half the luminosity, since the luminosity of the brightest galaxy in a group can account for over 50% of the total luminosity of the group. The derived parameters ($\log L_K$, $\log R_e$, and $\log \sigma_{200}$) for 94 systems of galaxies ($0.0038 < z < 0.09$) determine the Fundamental Plane (FP), which, with a scatter of 0.15, is similar in form to the FP of galaxy clusters obtained by Schaeffer et al. (1993) and D'Onofrio et al. (2013) with other methods and for different bands. We show that the FP in the near-infrared region (NIR) for 94 galaxy systems has the form of $L_K \propto R_e^{0.70\pm0.13}\sigma^{1.34\pm0.13}$, whereas in x-rays it has the form of—$L_X \propto R_e^{1.15\pm0.39}\sigma^{2.56\pm0.40}$. The form of the FP for groups and clusters is consistent with the FP for early-type galaxies determined in the same way. The form of the FP for galaxy systems deviates from the shape that one would expect from virial predictions. Adding the mass-to-light ratio as a fourth independent parameter has little effect on this deviation, but decreases the scatter of the FP for a sample of rich galaxy clusters by 12%.

DOI: 10.1134/S1990341316030019

Keywords: *galaxies:groups:general — galaxies:clusters:general — galaxies:fundamental parameters — galaxies:statistics*

1. INTRODUCTION

Dynamic and photometric properties of early-type galaxies (projected central radial velocity dispersion σ, effective radius R_e, and mean surface brightness $\langle I_e\rangle$) form the so-called Fundamental Plane (FP) [1–7]. The FP of galaxies has a significantly lower scatter compared to the Faber–Jackson relation [8] between the luminosity of a galaxy L and the central radial velocity dispersion σ for stars and the Kormendy relation [9] between the surface brightness of a galaxy L and its effective radius R_e obtained earlier. The FP for early-type galaxies is usually written with regard to the effective radius R_e which depends on the distance to the object:

$$\log R_e = a\,\log\sigma + b\,\log\langle I_e\rangle + c.$$

The coefficients a and b characterize the form of the FP, and c is the zero-point. The coefficient a usually varies within the range of 1.1–1.56, and b—within 0.75–0.90 for different bands and various methods of obtaining regression relations [10].

Since $\log R_e$ and $\log\langle I_e\rangle$ are determined by the luminosity of the galaxies—$\langle I_e\rangle = L/(2\pi R_e^2)$, the quantities $\log L$, $\log\sigma$, and $\log R_e$ also form a fundamental plane—$L \propto R_e^{\alpha}\,\sigma^{\beta}$. The type and form of the FP depend on the method used to determine these parameters and on the method used to calculate the regression between them. As shown in [11], the fundamental planes of all virialized objects (globular clusters, galaxies, galaxy clusters) are similar in form. If the studied galaxies are essentially virialized and homological systems with identical correlations between mass and luminosity, then $a = 2$ and $b = -1$ [7] or $\alpha = 1$ and $\beta = 2$ [12]. However, the observed FP coefficients differ from these values practically in all bands. They exhibit a deviation ("tilt"), possibly caused by structural inhomogeneity and properties of the stellar populations of galaxies (including the differences in M/L depending on the wavelength range) [10], or, by the differences in the portion of dark matter within the effective radius of the galaxies [13].

A galaxy cluster FP was first constructed based on the observed photometric properties of a sample of sixteen rich clusters of galaxies ($z < 0.2$) [14]. In that paper, the authors used V-band luminosities L and

*E-mail: flera@sao.ru

the effective radii of galaxy systems R_e containing half of the luminosity determined from a de Vaucouleurs profile. As a result of computing the regression dependence of L on other parameters, the following FP form was obtained: $L \propto R_e^{0.89\pm0.15}\sigma^{1.28\pm0.11}$. In [12], the parameters of 20 galaxy clusters (ENACS sample) were determined for different profiles: King, Hubble, NFW, and de Vaucouleurs. The best fit to the observed data was achieved with the King profile, for which the authors [12] derived the following FP: $L \propto R_e^{1.19\pm0.14}\sigma^{0.91\pm0.16}$.

For the WINGS [11] sample of galaxy clusters, V-band surface brightness profiles were constructed. Their central regions were approximated by de Vaucouleurs profiles, whereas the outer regions are best described by an exponential disk. The derived FP has the following form: (see Fig. 5 in [11]):

$$\log R_e = 1.08(\pm0.16)\ \log\sigma - 0.96(\pm0.13)\ \log\langle I_e\rangle + 2.60(\pm0.47).$$

The FP for galaxy clusters can be constructed not only from the observed data obtained in the visual range, but also from gas radiating in X-rays. As determined in [15], the FP of X-ray galaxy clusters is determined by the following parameters: $\log\rho_0$—central gas density, $\log R$—core radius, T—gas temperature.

Another representation of the FP is given in [16], where the authors used the optical luminosity, the radius containing half of it, and the X-ray luminosity for 78 galaxy clusters to construct the FP in the form of

$$\log L_{\rm opt}/L_\odot = \log(R_o^{0.84}\, L_x^{0.21}).$$

The aim of this work is to construct the FP and other dependences between the properties of 94 groups and clusters of galaxies with redshifts in the range of $0.012 < z < 0.09$ (and Virgo). The properties under study, L_K, σ, L_X, the effective radii derived from the luminosity and from the number of galaxies, and the correlations between them (FP) will allow us to determine the structural properties, the deviation from the relaxed state (evolutionary status), and estimate peculiar velocities and other properties of galaxy systems. The sample considered has 50 groups of galaxies with $\sigma < 400\,{\rm km\,s^{-1}}$ and 44 galaxy clusters with a larger radial velocity dispersion. Among these systems of galaxies, 45 represent the sample from [17] with measured X-ray luminosity; these objects were selected and observed homogeneously within the scope of the radial velocity surveys CfA2 and SSRS2. We have renamed the groups according to the name of the brightest galaxy or the corresponding name from the Abell catalog. Rich galaxy clusters are located mainly in the regions of galaxy superclusters Leo, Hercules, Corona Borealis, and Bootes. We have also included in our sample the rich X-ray clusters A 2029 and A 2142 in order to cover a large range of masses and X-ray luminosities.

The size of the galaxy systems, the number of galaxies, the luminosity and the (effective) radius within which half of the luminosity is radiated or half of the galaxies are contained, are determined from an integral distribution of the number of galaxies (based on the galaxy system profile) as a function of the squared radius from the center. This work has made use of the following databases: the SDSS[1] (Sloan Digital Sky Survey Data Release 7, 8) [18] catalog, the 2MASS[2] XSC (Two-Micron All-Sky Survey Extended Source Catalog) [19] catalog, and NED[3] (NASA Extragalactic Database). The paper is structured as follows. Section 2 describes the procedure of measuring the effective radius R_e, luminosity L_K, and number of galaxies N at that radius. The dependences between the properties o galaxy systems (Kormendy relation, Faber–Jackson relation, fundamental plane, and others) are derived and described in Section 3. The main results are listed in the Conclusion. The following cosmological parameters were used in this work: $\Omega_m = 0.3$, $\Omega_\Lambda = 0.7$, $H_0 = 70\,{\rm km\,s^{-1}\,Mpc^{-1}}$.

2. MEASURING THE OPTICAL PROPERTIES OF GALAXY SYSTEMS

2.1. Observed Properties of Galaxy Systems

Table 1 lists the coordinates of the galaxy system centers chosen by us, which usually coincide with the brightest galaxy in the system, and the X-ray luminosities with a link to the source. If the brightest galaxy is located apart from the rest, or there are several such galaxies, we used the galaxy centroid as the center (marked with an asterisk).

The results of determining the physical characteristics of part of the systems (63 galaxies) for the regions with the radii R_{200} and R_e are described and presented in [28, 29]. R_{200} is the radius within which the mass density of the systems exceeds the critical density of the Universe by a factor of 200 [30]; R_e is usually defined as the radius within which half of the luminosity of the galaxy systems is contained. The radial velocity dispersions σ_{200}, dynamical masses M_{200} and $M_{1/2}$, K_s-band luminosities (hereinafter, K, $L_{K,200}$, and $L_{K,1/2}$) are also given in the mentioned papers. The properties of the remaining third of

[1] http://www.sdss.org
[2] http://www.ipac.caltech.edu/2mass/releases/allsky/
[3] http://nedwww.ipac.caltech.edu

Table 1. X-ray luminosity of galaxy groups and clusters

Cluster	$RA_{J2000.0}$, deg	$Dec_{J2000.0}$, deg	$L_{0.1-2.4\ keV}$, 10^{44} erg s^{-1}	Cluster	$RA_{J2000.0}$, deg	$Dec_{J2000.0}$, deg	$L_{0.1-2.4\ keV}$, 10^{44} erg s^{-1}
Virgo	12.51373	12.39114	0.58[20]	NGC 6338	17.25638	57.41119	0.25[25]
HCG 042	10.00397	−19.63695	0.01[21]	NGC 3119	10.11441	14.37357	0.04[22]
HCG 062	12.88495	−9.20383	0.16[21]	NGC 5758	14.78391	13.66837	0.07[23]
AWM 3	14.47121	25.84877	–	A 2199	16.47729	39.55123	1.89[20]
NGC 2563	8.34325	21.06780	0.05[21]	NGC 6107	16.29459	35.00422	0.17[25]
AWM 7	2.90760	41.57959	–	AWM 4	16.08407	23.93269	0.22[20]
MKW 01s	9.33394	1.03829	–	A 1177	11.16235	21.75894	0.11[20]
NGC 0533	1.42538	1.75911	0.07[22]	NGC 3847*	11.75626	33.34110	–
NGC 0741	1.93918	5.62894	0.04[23]	A 1185*	11.17818	28.70554	0.15[25]
NGC 0080	0.35301	22.35712	0.07[22]	A 2063	15.38481	8.60922	1.04[20]
MKW 12	14.04684	9.34138	–	A 2052	15.27902	7.02163	1.29[20]
MKW 04	12.07418	1.89597	–	AWM 5	16.96614	27.85442	–
MKW 01	10.00840	−2.9690	–	A 1228A	11.36181	34.36278	–
MKW 10*	11.70171	10.29136	0.02[24]	A 2147	16.03806	15.97746	1.45[20]
NGC 3022	9.82757	−5.16658	–	A 2151*	16.08570	17.71912	0.45[20]
NGC 2783	9.22763	29.99296	–	NGC 5098	13.33742	33.14341	0.13[20]
UGC 07115	12.13488	25.23710	0.04[22]	A 1139	10.96972	1.60458	0.15[20]
UGC 02005	2.53271	1.24652	0.04[22]	A 1228B	11.38235	34.11149	0.06[25]
IC 5357	23.78972	−2.30067	0.03[22]	A 1983	14.88203	16.70286	0.24[20]
NGC 2965	9.72199	36.24782	–	MKW 03s	15.36440	7.70882	1.37[20]
NGC 1016	2.63877	2.11925	–	A 0671	8.47546	30.43113	0.46[20]
NGC 3158	10.23070	38.76490	0.03[22]	A 0757	9.21882	47.70839	0.46[20]
NGC 0070	0.30625	30.06667	0.09[23]	RXC J1022	10.36951	38.51782	0.18[20]
UGC 07132	12.15273	1.56951	–	A 1991	14.90875	18.64232	0.70[20]
AWM 2	12.26044	23.98194	–	A 0602	7.89072	29.35944	0.58[20]
NGC 5171	13.48932	11.73511	0.10[23]	A 1781*	13.74597	2.74565	–
NGC 2832	9.32968	33.74974	0.10[23]	A 1795	13.81458	26.59293	5.75[20]
A 1656	13.00226	27.97694	3.70[20]	A 1275	11.50088	36.63722	0.22[25]
NGC 5129	13.40278	13.97654	0.09[23]	A 1825	13.96757	20.61902	0.11[25]
NGC 1132	2.88107	−1.27476	0.10[22]	A 1828E*	13.97076	18.34617	–
SS2b 164	11.37884	−7.67625	0.04[22]	A 1828W	13.93856	18.29288	–
NGC 7436B	22.96598	26.14994	–	A 2124	15.74973	36.10946	0.69[20]
NGC 5306	12.81983	−7.22440	0.05[22]	A 2079	15.46253	28.92873	0.37[26]
NGC 5223	13.57367	34.69043	0.06[23]	A 2092	15.55427	31.14515	0.40[26]
MKW 05	14.01033	−2.85782	–	A 2065	15.37477	27.70763	2.52[20]
NGC 7385	22.83183	11.60857	0.06[22]	A 0744	9.12236	16.65189	0.39[20]
NGC 4325	12.38519	10.62124	0.15[21]	A 2067	15.38561	30.87750	0.44[20]
IC 0186	2.93118	9.311830	0.02[22]	A 2089	15.54717	28.03951	–
NGC 7237	22.24611	13.84167	0.06[23]	A 1238	11.38176	1.11441	0.26[25]
IC 2476	9.46467	29.98575	–	A 1775B	13.69698	26.37347	1.60[27]
NGC 5627	14.47619	11.37824	0.02[22]	A 1800	13.82321	28.10731	1.56[20]
MKW 08	14.67857	3.46542	0.31[20]	RXC J1350	13.83765	29.22148	–
UGC 05088	9.55714	34.04809	0.02[25]	A 2061	15.35572	30.67094	2.02[20]
MKW 04s	12.11083	28.17447	–	A 2029	15.18225	5.74478	7.80[20]
NRGb 004	8.63520	25.27261	0.18[23]	A 1898*	14.34415	25.25784	0.11[26]
AWM 1	9.28526	20.06970	–	A 2019	15.05800	27.15445	0.15[26]
NGC 2795	9.26776	17.62837	0.05[25]	A 2142	15.97222	27.23341	10.58[20]

the galaxy systems are determined in this work using the same method as in [28, 29]. The masses M_{200} and $M_{1/2}$ were determined from the radial velocity dispersion σ_{200} of the galaxies as $M \propto \sigma^3$ and $M \propto \sigma^2$ in accordance with the methods described in these papers, assuming that the systems are in a state of virial equilibrium and have isotropic radial velocities.

To characterize in more detail the observed structure and kinematics of the galaxy groups and clusters studied in this work, as well as their nearby surroundings, we show in Fig. 1 and Fig. 2, using the example of clusters A 1800 and A 2124, the following:

1) the radial velocity scatter for cluster members, as well as for galaxies which deviate by more than 2.7σ and are classified as background galaxies, as a function of the squared distance to the center of the cluster (the top left panel in the figure);

2) the integral distribution of the number of galaxies as a function of the squared radius, to reveal the dense cluster core, the more sparse halo, and the outer region, where the distribution becomes linear in the chosen coordinates, i.e. a uniform (on average) distribution of surrounding galaxies is observed (the bottom left panel);

3) the image plane projection of galaxies in equatorial coordinates (the top right panel);

4) the histogram of the radial velocity distribution for all the galaxies within the radius R_{200} (the solid curve indicates a Gaussian function corresponding to the radial velocity dispersion of the clusters in Table 1) (the bottom right panel).

Early-type galaxies were selected based on their SDSS r-band characteristics: fracDeV ≥ 0.8, where fracDeV shows the contribution of the bulge to the surface brightness profile of a galaxy; $r_{90}/r_{50} \geq 2.6$, where $c = r_{90}/r_{50}$ is the concentration index equal to ratio of the radii which confine 90% and 50% of the Petrosian flux. Additionally, we restricted the $(u-r)$ colors: $\Delta(u-r) > -0.2$. In Fig. 1 and Fig. 2, early-type galaxies are denoted by circles with dots inside.

2.2. Determining the Size and Effective Radius of Galaxy Systems

The break in the cluster profile which represents the distribution of the number of galaxies as a function of the squared radius from the selected center, shown in the bottom left panels in Fig. 1 and Fig. 2, can be used to determine with sufficient accuracy the size of the system, its virialized part with the radius R_h (the dashed-and-dotted line), and the cluster core of radius R_c (long-dashed line). The figures also show the region of radius R_{200} (short-dashed line). The number of galaxies increases sharply in the central parts of a group or cluster (this region is restricted by the radius R_c); the straight line shows the region of constant density increase. We call this region the cluster halo. It includes galaxies and small groups which got there only recently. The radius R_h of this region usually exceeds R_{200} and is close to the radius $R_{100} \approx 1.3R_{200}$ [31], within which the systems are also considered to be virialized. Another straight line shows the region of constant density increase beyond the virialized part of the systems. This method of determining the size of galaxy systems was developed by us for the first time. We used it on a sample of galaxy clusters with known masses measured from gas radiating in the X-ray range [29]. In this work, we have additionally refined the R_h radii for the rich galaxy clusters A 1656 and A 1795, since they were underestimated in [29].

As shown in the bottom left panels in Fig. 1 and Fig. 2, N_1 galaxies (excluding the background) are contained within the R_h radius (or N_{1c} galaxies if the background is taken into account), which we found graphically using the slope of the galaxy distribution beyond the virialized cluster region. Despite the fact that we had already selected the members of galaxy groups based on the radial velocities, according to [32], they might include background galaxies, the so-called "interlopers". N_1 and N_{1c} are related as $N_{1c} = N_1 - \pi R_h^2 \Sigma^N$, where the density of the galaxies (in the R_h region) is $\Sigma^N = (N_1 - N_{1c})/(\pi R_h^2)$. For the derived N_{1c} galaxies we have measured the luminosity $L_{1c} = L_1/N_1 N_{1c}$, found the cluster radius $R_e(L_{1c}/2)$ (hereinafter, $R_e(L/2)$) within which half of the system's luminosity is contained, and used $N_{1c}/2$—$R_e(N_{1c}/2)$ (hereinafter $R_e(N/2)$) to determine the radius which contains half of the total number of galaxies in the system.

To construct the classical FP based on optical observations, one needs to find the luminosity of the system, and determine the effective radius containing half of it. As mentioned above, in [28, 29] we determined the NIR luminosity of galaxy clusters in the K band. To that end, we used the results of galaxy photometry presented in the final version of the 2MASS catalog of extended sources—XSC [19]. We increased the photometric limit of this catalog to $K = 14\overset{\text{m}}{.}7{-}15\overset{\text{m}}{.}0$, taking into account the $(r-K)$-color dependence of a galaxy on the SDSS color $(u-r)$. Since our sample also contains distant galaxy clusters, the total luminosity for systems with $z > 0.035$ was determined as a sum of luminosities of all the observed galaxies with an additional component (up to $M_K = -21^{\text{m}}$), obtained from the composite luminosity function of the galaxy clusters using the method described in [33].

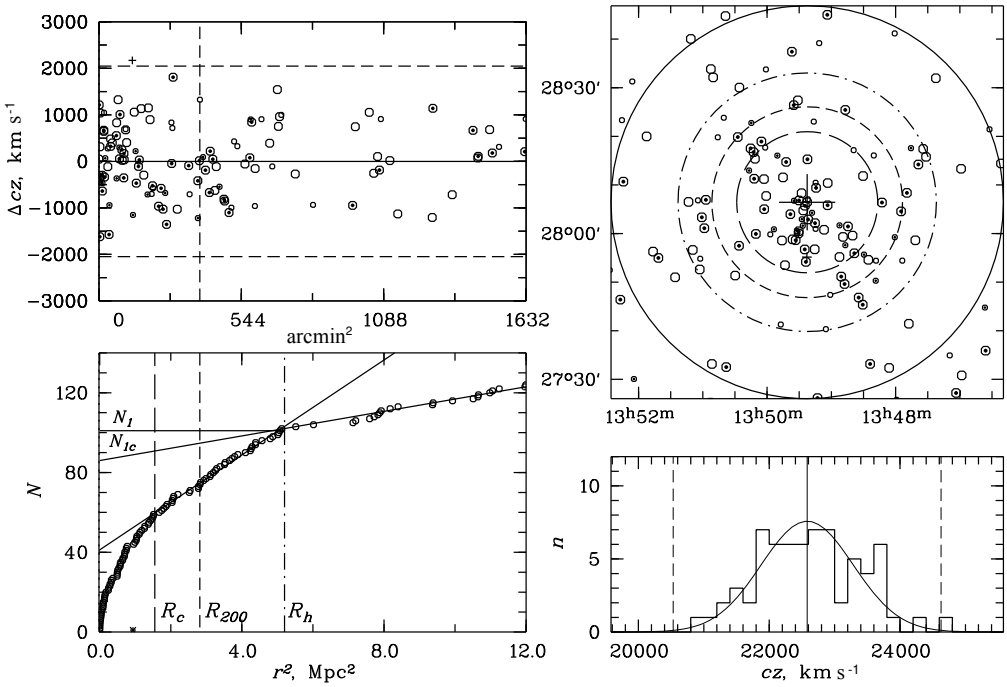

Fig. 1. Distribution of galaxies in the A 1800 cluster. Top left: deviation of radial velocities of galaxies from the mean radial velocity of the cluster, determined for the galaxies within the radius R_{200}. The horizontal dashed lines correspond to the deviations of $\pm 2.7\sigma$, the vertical dashed line marks the radius R_{200}. The larger circles mark galaxies brighter than $M_K^* + 1 = -23\overset{\text{m}}{.}29$, circles with a dot mark early-type galaxies, and the plus marks a background galaxy. The horizontal axis shows the distance from the center of the cluster in squared arcminutes. Bottom left: integral distribution of the number of galaxies as a function of the squared distance from the center of the cluster in megaparsecs. The vertical lines show, besides the radius R_{200}, the radius R_h (the dashed-and-dotted line), and the radius R_c (long-dashed line). The circles correspond to the galaxies shown by circles in the top left panel, the stars represent the background galaxies. Top right: sky distribution of the galaxies shown in the top left panel in equatorial coordinates (the designations are the same). The circles show regions with the radii R_{200}, R_h, and R_c. The region under investigation is limited to a circle of $40'$ radius. The large cross marks the center of the cluster. Bottom right: radial velocity distribution for all galaxies within the radius R_{200} (the solid curve shows (for the members of the cluster) the Gaussian function corresponding to the cluster σ). The solid vertical line shows the mean radial velocity of the cluster, the dashed lines correspond to $\pm 2.7\sigma$ deviations.

2.3. Relation between K-Luminosity and the Number of Galaxies in Galaxy Systems

As a result of the study of nine rich galaxy clusters, a practically linear dependence was found to exist between the number of galaxies within the radius R_{200} and their NIR luminosity, mainly due to the fact that the luminosity function for galaxy clusters in the region of bright galaxies varies little from cluster to cluster [34]. In Fig. 3 we present this dependence for our sample of galaxy groups and clusters ($N = 191$) to show that the effective radius for the groups (especially) and clusters of galaxies can be defined as the radius containing half the system galaxies. The R_e radii derived this way are, on the average, bigger by 17%.

A very bright galaxy (the brightest in the system) is usually located at the center of galaxy groups and clusters. Its luminosity can exceed 50% of the total luminosity of the system. For fourteen such galaxy groups in our sample, e.g. AWM 04 and A 1177 ("fossil" galaxy groups), with a very bright galaxy in the center, we determined $R_e(L/2)$ from the luminosity derived by subtracting the luminosity of the brightest galaxy from the total luminosity, and $R_e(N/2)$—using the usual method including all the galaxies. With this in mind, in this work we determined the effective radii of galaxy systems in two ways, as radii containing half the luminosity $L/2$ and half of the total number of galaxies $N/2$; however, the second method is preferable for galaxy groups and clusters when constructing the overall fundamental plane. The first method is needed to search for greatly evolved (fossil)

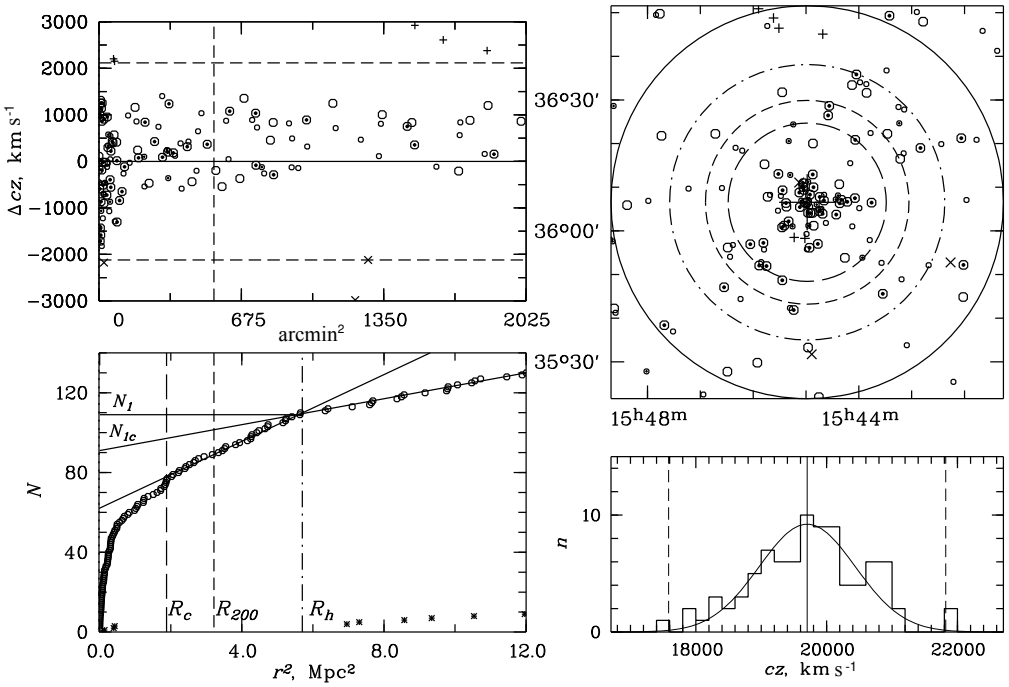

Fig. 2. Distribution of galaxies in the A 2124 cluster. The crosses in the top left panel show the foreground galaxies. The structure and designations are the same as in Fig. 1. The region under investigation is limited to a circle of 45′ radius.

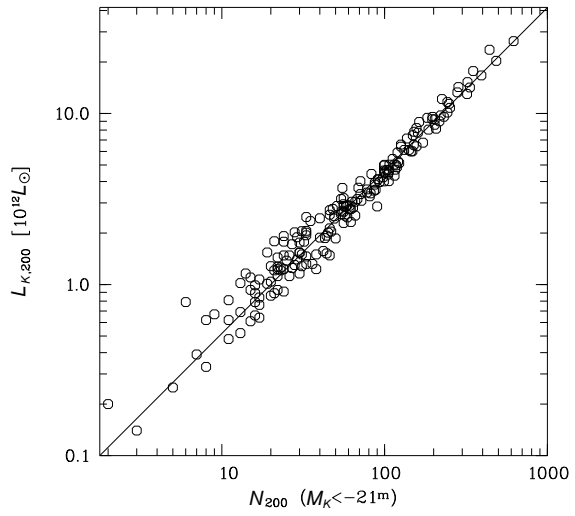

Fig. 3. Luminosity of galaxy groups and clusters in the K band ($M_K < -21^{\rm m}$) as a function of the number of galaxies within the R_{200} radius. The solid line shows the linear dependence $L_{K,\,200} \propto N_{200}$.

groups, where the brightest galaxy had accumulated a gigantic luminosity absorbing the smaller galaxies.

In Table 2 we present the results of our measurements of the physical properties of the galaxy groups and clusters under study (sorted according to redshift) for the region of radius R_{200}, as well as effective radii R_e, derived from half the luminosity $L/2$ and half the number of galaxies $N/2$. The table columns give: (1)—name of the system (the galaxy groups from [17] are named after the brightest galaxy), (2)—heliocentric redshift, (3)—R_{200} radius in Mpc, (4)—R_c radius in Mpc, (5)—R_h radius in Mpc, (6)—radial velocity dispersion with the cosmological correction $(1+z)^{-1}$ within R_{200} σ_{200} (hereinafter simply σ), (7)—mass M_{200}, (8)—IR-luminosity $L_{K,\,200}$ ($M_K < -21^{\rm m}$) within R_{200}, (9)—IR-luminosity $L_{K,\,1}$=$L_{1c}/2$ ($M_K < -21^{\rm m}$) and in column (10)—the effective radius $R_{e,\,L}$=$R_e(L/2)$ in Mpc containing this luminosity, (11)—IR-luminosity $L_{K,\,2}$ radiated by $N_{1c}/2$ galaxies and in (12)—the effective radius $R_{e,\,N}$=$R_e(N/2)$ in Mpc containing this luminosity. The mass measurement errors correspond to the errors of measuring σ and are defined as the errors of function $y = \sigma^3$, $S_y = 3\sigma^2/\sqrt{(}N)\,S_\sigma$ for M_{200}. The asterisks denote the galaxy groups for which $R_e(L/2)$ is determined with the subtraction of the luminosity of the brightest galaxy. Similar data for the 29 galaxy systems reported in [29] are not included in Table 2.

Table 2. Physical properties of galaxy groups and clusters

Cluster	z_h	R_{200}, Mpc	R_c, Mpc	R_h, Mpc	σ_{200}, km s^{-1}	M_{200}, $10^{14}M_\odot$	$L_{K,200}$, $10^{12}L_\odot$	$L_{K,1}$, $10^{12}L_\odot$	$R_{e,L}$, Mpc	$L_{K,2}$, $10^{12}L_\odot$	$R_{e,N}$, Mpc
(1)	(2)	(3)	(4)	(5)	(6)	(7)	(8)	(9)	(10)	(11)	(12)
HCG 042*	0.01259	0.56	0.30	0.75	228	0.20 ± 0.15	0.62	0.34	0.28	0.56	0.26
HCG 062	0.01434	1.00	0.39	1.03	407	1.16 ± 0.56	2.05	0.56	0.49	0.39	0.34
AWM 3*	0.01488	0.66	0.44	1.04	269	0.33 ± 0.18	0.48	0.22	0.16	0.45	0.42
NGC 2563	0.01570	0.91	0.28	1.00	369	0.86 ± 0.39	1.40	0.66	0.27	0.73	0.34
AWM 7	0.01734	1.71	1.07	1.96	698	5.84 ± 1.51	4.13	1.75	0.40	1.88	0.52
MKW 01s*	0.01756	0.44	0.35	0.68	179	0.10 ± 0.10	0.25	0.11	0.15	0.22	0.32
NGC 0533	0.01841	0.99	0.59	1.45	404	1.13 ± 0.74	1.79	0.80	0.32	1.24	0.39
NGC 0741*	0.01842	0.90	0.62	0.98	368	0.86 ± 0.41	1.27	0.59	0.27	1.03	0.34
NGC 0080	0.01910	0.73	0.37	0.79	296	0.44 ± 0.23	1.94	0.96	0.23	1.21	0.28
MKW 12	0.01976	0.47	0.42	1.10	192	0.12 ± 0.07	0.99	0.62	0.26	0.90	0.42
MKW 04	0.02021	1.26	0.83	1.51	515	2.34 ± 0.74	2.56	1.24	0.27	1.90	0.48
MKW 01	0.02079	0.79	0.42	0.69	323	0.58 ± 0.44	0.75	0.34	0.13	0.48	0.15
MKW 10*	0.02083	0.36	0.15	0.60	147	0.05 ± 0.05	0.79	0.42	0.10	0.76	0.12
NGC 3022	0.02096	0.68	0.73	1.14	276	0.36 ± 0.28	0.93	0.61	0.35	0.69	0.46
NGC 2783	0.02215	0.85	0.90	1.33	346	0.71 ± 0.38	1.10	0.50	0.39	0.67	0.43
UGC 07115	0.02220	0.82	0.66	1.06	334	0.64 ± 0.26	1.32	0.84	0.57	0.73	0.52
UGC 02005	0.02234	0.86	0.73	1.12	352	0.75 ± 0.34	1.12	0.58	0.55	0.73	0.66
IC 5357	0.02244	0.93	0.57	1.02	381	0.95 ± 0.62	1.21	0.58	0.38	0.56	0.36
NGC 2965	0.02247	0.42	0.41	1.18	173	0.09 ± 0.10	0.39	0.23	0.16	0.30	0.32
NGC 1016*	0.02258	0.79	0.36	1.10	322	0.57 ± 0.38	1.92	0.78	0.35	1.16	0.26
NGC 3158	0.02263	0.92	0.26	1.08	375	0.90 ± 0.44	1.78	0.87	0.16	1.37	0.26
NGC 0070	0.02264	1.02	0.62	1.15	415	1.22 ± 0.65	2.01	0.95	0.12	1.16	0.36
UGC 07132*	0.02272	0.38	0.44	0.71	156	0.06 ± 0.06	0.20	0.14	0.64	0.18	0.37
AWM 2	0.02276	0.72	0.42	0.77	293	0.43 ± 0.24	0.93	0.42	0.15	0.49	0.31
NGC 5171	0.02300	0.91	0.84	1.44	371	0.88 ± 0.37	1.50	1.03	0.64	0.94	0.52
NGC 2832	0.02304	0.81	0.69	1.23	331	0.62 ± 0.24	1.76	0.86	0.24	1.18	0.46
NGC 5129	0.02340	0.71	0.77	1.36	290	0.42 ± 0.22	1.28	0.65	0.24	0.94	0.43
NGC 1132*	0.02351	0.51	0.53	1.05	210	0.16 ± 0.13	0.62	0.37	0.50	0.56	0.28
SS2b 164	0.02381	0.82	0.60	1.56	334	0.64 ± 0.43	1.04	0.84	0.58	0.93	0.60
NGC 7436B*	0.02472	0.94	0.42	1.09	383	0.96 ± 0.54	1.72	0.75	0.26	1.16	0.40
NGC 5306*	0.02473	0.75	0.56	1.63	305	0.48 ± 0.42	1.16	0.71	0.52	0.43	0.52
NGC 5223	0.02483	0.66	0.57	0.97	271	0.34 ± 0.19	1.54	0.59	0.20	1.02	0.50
MKW 05*	0.02486	0.70	0.63	0.88	288	0.41 ± 0.27	0.69	0.37	0.11	0.61	0.39
NGC 7385	0.02511	1.14	0.55	0.85	466	2.24 ± 1.40	2.40	1.08	0.17	1.64	0.34
NGC 4325	0.02539	0.66	0.41	0.84	271	0.34 ± 0.26	0.61	0.34	0.17	0.44	0.32
IC 0186	0.02602	0.78	0.69	1.16	318	0.55 ± 0.48	1.26	0.72	0.44	0.89	0.50
NGC 7237	0.02610	0.92	0.78	1.47	376	0.91 ± 0.38	1.57	0.95	0.44	1.06	0.50
IC 2476	0.02620	0.59	0.59	0.96	243	0.24 ± 0.16	0.76	0.40	0.18	0.53	0.39
NGC 5627	0.02668	0.77	0.53	1.10	314	0.53 ± 0.28	1.38	0.74	0.46	0.69	0.44

Table 2. (Cont.)

Cluster	z_h	R_{200}, Mpc	R_c, Mpc	R_h, Mpc	σ_{200}, km s^{-1}	M_{200}, $10^{14}M_\odot$	$L_{K,200}$, $10^{12}L_\odot$	$L_{K,1}$, $10^{12}L_\odot$	$R_{e,L}$, Mpc	$L_{K,2}$, $10^{12}L_\odot$	$R_{e,N}$, Mpc
(1)	(2)	(3)	(4)	(5)	(6)	(7)	(8)	(9)	(10)	(11)	(12)
MKW 04s	0.02793	1.03	0.82	1.49	423	1.29 ± 0.51	1.88	0.97	0.29	1.46	0.55
NRGb 004	0.02809	0.88	0.78	1.13	362	0.81 ± 0.44	1.30	0.65	0.51	0.63	0.48
AWM 1	0.02865	0.98	0.64	1.05	402	1.11 ± 0.48	2.35	0.99	0.35	1.31	0.40
NGC 2795	0.02899	1.04	0.71	1.32	431	1.37 ± 0.55	2.39	1.20	0.25	1.42	0.38
NGC 3119	0.02966	0.87	0.91	1.83	355	0.76 ± 0.38	1.54	1.17	0.56	1.26	0.62
NGC 5758	0.02992	0.71	0.66	1.09	291	0.42 ± 0.20	1.23	0.68	0.20	0.79	0.40
NGC 6107	0.03109	1.33	0.99	1.86	546	2.78 ± 0.82	3.58	1.90	0.50	2.23	0.65
NGC 3847	0.03246	0.91	0.86	1.66	372	0.88 ± 0.34	2.58	1.39	0.66	1.65	0.77
A 1185	0.03273	1.69	1.38	2.01	676	5.27 ± 1.20	6.85	3.00	0.55	3.38	0.66
A 1228A	0.03506	0.57	0.47	1.06	216	0.17 ± 0.11	1.52	1.02	0.34	1.41	0.47
A 1228B	0.04289	0.84	0.66	1.11	347	0.71 ± 0.40	1.78	0.88	0.12	1.05	0.20
A 0671	0.04980	1.95	1.82	2.41	805	8.83 ± 2.47	7.72	3.82	0.44	4.56	0.61
A 0757	0.05132	0.89	0.77	1.79	368	0.84 ± 0.42	2.70	1.54	0.50	1.63	0.56
A 0602	0.06055	1.35	1.32	1.86	560	2.96 ± 1.16	4.33	2.44	0.72	2.56	0.74
A 1781	0.06226	0.87	0.87	1.56	362	0.80 ± 0.48	2.77	2.09	0.84	2.01	0.83
A 1825	0.06327	1.52	0.71	1.38	633	4.26 ± 2.02	3.60	1.77	0.25	2.14	0.40
A 1828E*	0.06358	0.80	0.32	0.82	335	0.63 ± 0.52	0.89	0.37	0.25	0.65	0.28
A 1828W	0.06395	0.50	0.36	0.92	207	0.15 ± 0.13	1.39	0.95	0.17	1.15	0.29
A 2124	0.06572	1.77	1.37	2.39	736	6.70 ± 2.18	6.75	3.93	0.50	4.38	0.60
A 2079	0.06575	1.48	1.35	2.12	618	3.96 ± 1.29	8.92	4.97	0.60	6.12	0.91
A 2067	0.07294	0.68	0.49	1.11	286	0.39 ± 0.31	0.91	0.73	0.36	0.78	0.46
A 2089	0.07355	1.27	0.91	1.48	531	2.50 ± 1.05	4.53	2.39	0.59	2.78	0.63
RXC J1350	0.07644	0.86	0.41	1.30	359	0.77 ± 0.48	2.53	1.62	0.39	1.63	0.46
A 2061	0.07775	1.70	1.37	1.95	712	6.03 ± 1.65	13.29	6.60	0.51	7.82	0.65
A 1898	0.07852	1.04	0.81	1.90	434	1.36 ± 0.89	2.95	2.05	0.61	2.42	0.64
A 2019	0.08118	0.82	0.59	1.22	345	0.68 ± 0.50	1.87	1.54	0.52	1.40	0.45

3. CONSTRUCTING THE FUNDAMENTAL PLANE AND OTHER SCALING RELATIONS FOR GALAXY GROUPS AND CLUSTERS

3.1. Dependences between L_K–R_e, L_K–σ and the NIR Fundamental Plane

Fig. 4 shows the L_K–R_e dependence (for $L_K/2\pi R_e^2$ we practically get the Kormendy relation) for the studied galaxy systems for which the effective radius R_e was found in two ways as the radius containing $L/2$ luminosity or $N/2$ galaxies. In the left panel of Fig. 4 the shown dependence (for the case of $N/2$) has the form of $L_K \propto R_e^{1.62\pm0.15}$ and is in accordance with the results presented in, e.g., [35] and [14]. For the $L/2$ case we have also obtained a regression dependence, shown along with all the other relations for this case in Table 3. This table gives, in the first column, the number of galaxy systems included in the regression; the second column gives the variable with regard to which the regression was performed, and columns (3) and (4) show the results obtained for R_e derived from $N/2$ and from $L/2$. The "fossil" groups in the figures are shown by filled circles, the regression relations were computed without them. The three poorest groups with $\sigma < 200$ km s^{-1} deviate the most. The Faber–Jackson relation for our sample also agrees within the margin of error with the data of [35] and [14] and has the form of

$$L_K(N/2) \propto \log \sigma^{1.79\pm0.11}.$$

To be able to compare the obtained results of constructing the cluster FP with the results of other

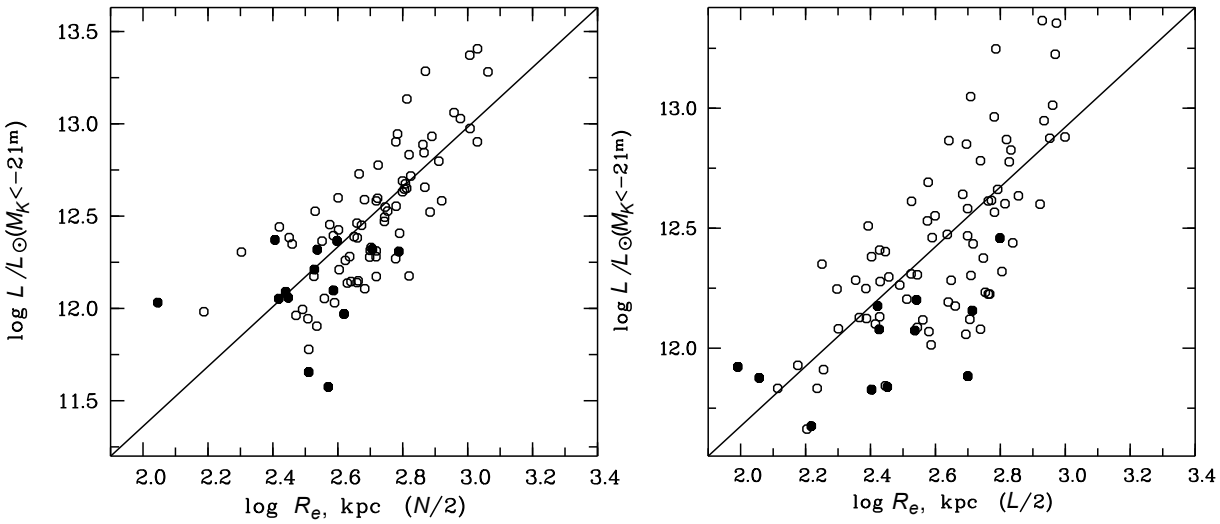

Fig. 4. The $L_K{-}R_e$ dependence for galaxy groups and clusters based on two ways of determining R_e: as half of the galaxies (left), and half the luminosity (right). The filled circles show the groups for which the radius $R_e(L/2)$ was determined with the subtraction of the luminosity of the brightest galaxy. The regression relations have the form of $L_K \propto R_e^{1.62\pm0.15}(N/2)$ and $L_K \propto R_e^{1.24\pm0.13}(L/2)$.

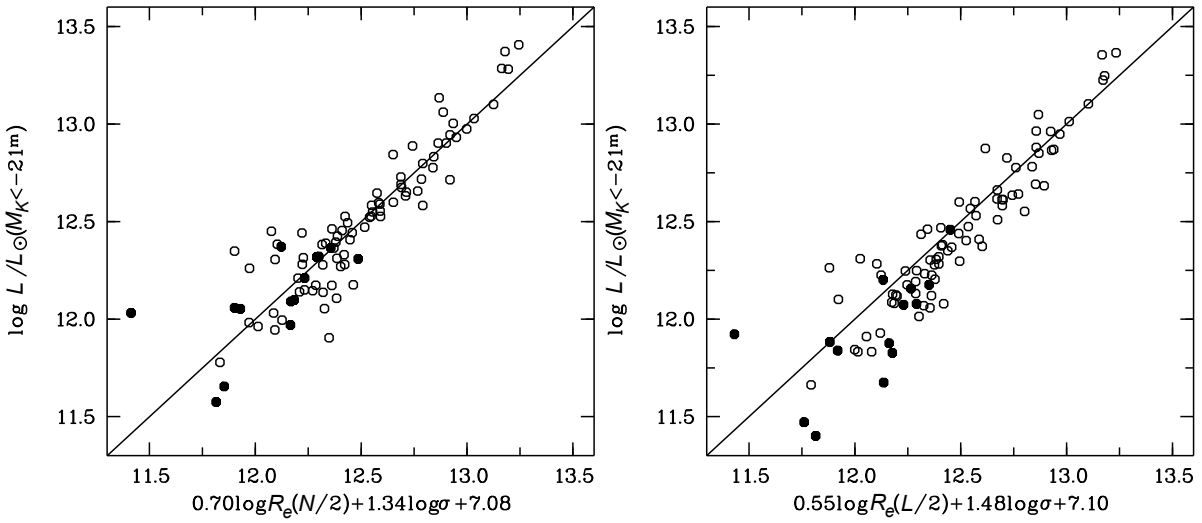

Fig. 5. Fundamental plane of galaxy groups and clusters in the NIR range. The filled circles show the groups for which the radius $R_e(L/2)$ was estimated with the subtraction of the luminosity of the brightest galaxy. The regression relations have the form of $L_K \propto R_e^{0.70\pm0.13}(N/2)\sigma^{1.34\pm0.13}$ and $L_K \propto R_e^{0.55\pm0.09}(L/2)\sigma^{1.48\pm0.11}$.

authors (e.g., [14]), we took $\log L_K$, $\log R_e$, $\log\sigma$ and found a regression relation with regard to $\log L_K$. In our study, $\log L_K$ is the K-band luminosity of galaxy systems (for the same limit $M_K = -21^{\rm m}$) in $L_\odot$, $\log R_e$ is the effective radius of the system in kpc, which contains either half of the total number of galaxies ($N/2$) found from the profile described above, or half the luminosity ($L/2$). Unlike the FP for early-type galaxies, where the central dispersion of stellar radial velocities is considered, for galaxy clusters and groups it is better to use the radial velocity dispersion of galaxies within the virialized region (in our case we took σ_{200} within R_{200}) as the most accurate, since accuracy depends on the number of galaxies used.

Fig. 5 shows the FP for our sample of 94 galaxy groups and clusters in the following form:

$$\begin{aligned}\log L_K(N/2) &= 0.70(\pm0.13)\log R_e(N/2)\\ &+ 1.34(\pm0.13)\log\sigma + 7.08(\pm0.15)\end{aligned}$$

Table 3. Scaling relations between the properties of galaxy groups and clusters

N	Direction	$N/2$	$L/2$
80	L_K	$R_e^{1.62\pm0.15}$	$R_e^{1.24\pm0.13}$
80	L_K	$\sigma^{1.79\pm0.11}$	$\sigma^{1.88\pm0.11}$
80	L_K	$R_e^{0.70\pm0.13}\,\sigma^{1.34\pm0.13}$	$R_e^{0.55\pm0.09}\,\sigma^{1.48\pm0.11}$
24	L_K	$R_e^{0.76\pm0.18}\,\sigma^{1.60\pm0.16}$	$R_e^{0.82\pm0.11}\,\sigma^{1.66\pm0.12}$
24	L_K	$R_e^{0.74\pm0.15}\,\sigma^{1.69\pm0.14}\,(M_X/L_K)^{0.28\pm0.10}$	$R_e^{0.80\pm0.10}\,\sigma^{1.72\pm0.11}\,(M_X/L_K)^{0.18\pm0.10}$
63	L_K	$R_e^{0.81\pm0.21}\,L_X^{0.30\pm0.05}$	$R_e^{0.57\pm0.13}\,L_X^{0.36\pm0.04}$
63	L_X	$R_e^{1.15\pm0.39}\,\sigma^{2.56\pm0.40}$	$R_e^{0.46\pm0.28}\,\sigma^{3.06\pm0.36}$

and, taking into account $\langle I_e\rangle = L_K/(2\pi R_e^2)$,

$$\log R_e(N/2) = 1.03(\pm0.10)\log\sigma - 0.77(\pm0.10)\log\langle Ie\rangle + 4.83(\pm0.11).$$

The FP constructed by us agrees within the errors with the results of [11, 12, 14], where the authors use other methods to determine the effective radius of galaxy systems: R_e is determined either by fitting a de Vaucouleurs profile to the surface brightness (luminosity) profile, or by using other profiles (e.g., Hubble, King).

3.2. X-ray Fundamental Plane

For another baryonic component of systems of galaxies—gas, we have obtained the following FP by changing the K-band luminosity to the luminosity of gas in the X-ray range:

$$\log L_X = 1.15(\pm0.39)\log R_e(N/2) + 2.56(\pm0.40)\log\sigma + 33.34(\pm0.36),$$

where L_X is the X-ray luminosity. The scatter of the derived fundamental plane, shown in Fig. 6, is 2.5 times larger than that of the FP for the stellar population of galaxy systems. We should note that while the $\log R_e$ coefficients for both fundamental planes are in agreement with each other within the errors, the $\log\sigma$ coefficient for the X-ray FP is significantly larger and close to virial predictions.

We have also constructed a fundamental plane similar to the one derived in [16], between the optical luminosity, the effective radius found from this luminosity, and the X-ray luminosity

$$\log L_K = 0.81(\pm0.21)\log R_e(N/2) + 0.30(\pm0.05)\log L_X - 2.77(\pm0.19),$$

which agrees within the errors with the authors' results for 78 galaxy clusters.

3.3. Comparison of the FP of Galaxy Systems with the FP for Early-Type Galaxies

In Fig. 7 we show the FP for galaxy groups and clusters together with the FP for early-type galaxies. To this end, we converted the L_K-luminosities of galaxy systems, taking into account the color $(r-K)\sim3$, to r-band luminosities (SDSS)—L_r. We took the rounded value of color $(r_{\rm pet}-K)$, calculated for our sample: the mean system color varies in the 2.5–3.0 interval. The early-type galaxies were selected earlier from the SDSS (DR8) catalog, when we were determining peculiar velocities in superclusters. The description of the selection criteria and the results obtained for the superclusters Hercules and Leo are reported in [36]. The FP of 2111 early-type galaxies is determined, as in the case of galaxy clusters, by a regression with regard to L_r. We can note that the forms of fundamental planes for both galaxies and galaxy systems are in good agreement with each other, and the zero-points differ more strongly than reported in [11]. The authors of the mentioned paper suggest that the differences in coefficients and zero-points derived by them are due, in all likelihood, to either different amounts of dark matter within R_e for galaxy clusters, or to the unaccounted for luminosity of their inner environment. For the galaxy systems under study, we find that increasing the galaxy luminosity by, e.g., 50%, does not increase significantly their zero-point. The zero-point of the FP for galaxy groups and clusters increases if we take into account the mass-to-light ratio as a fourth parameter, as shown below.

3.4. FP of Galaxy Systems with Consideration for Their Mass-to-Light Ratio

According to [37], the expression $L = SR_dL/MR\sigma^2$ should be true for virialized systems, where the S parameter belongs to the inner structure of the object and R_d demonstrates the degree of the system's

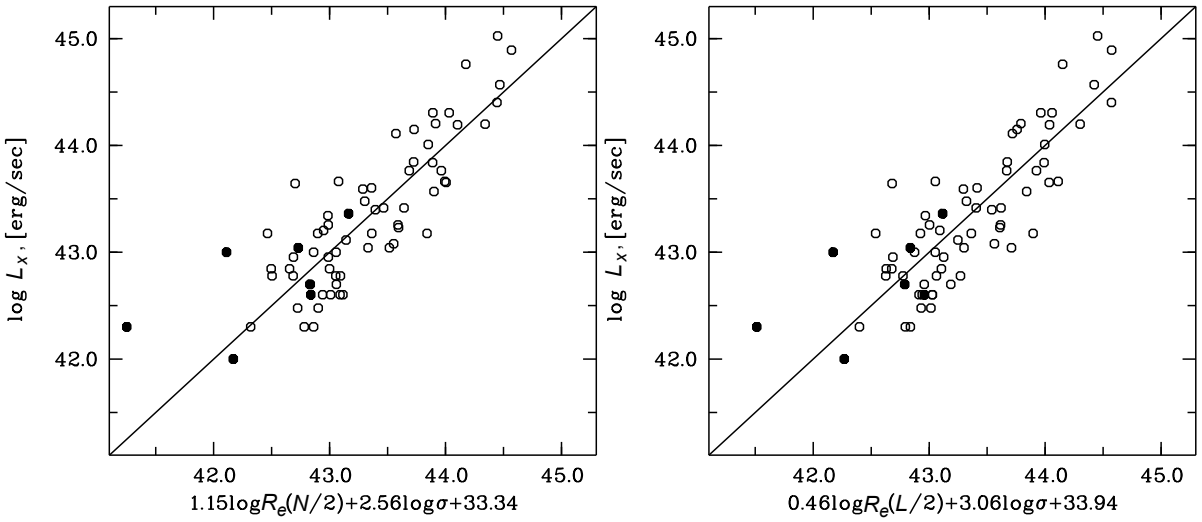

Fig. 6. Fundamental plane for galaxy groups and clusters in the X-ray range. The filled circles show the groups for which the $R_e(L/2)$ radius was estimated with the subtraction of the luminosity of the brightest galaxy. The regression relations have the form of $L_X \propto R_e^{1.15\pm0.39}(N/2)\sigma^{2.56\pm0.40}$ and $L_X \propto R_e^{0.46\pm0.28}(L/2)\sigma^{3.06\pm0.36}$.

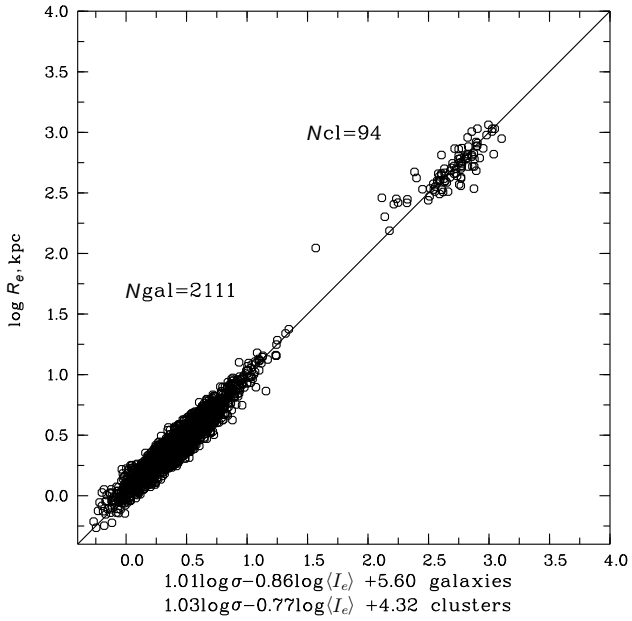

Fig. 7. Fundamental plane for galaxies and galaxy groups and clusters vs. the long axis log R_e. The R_e radius for galaxy systems is determined as the radius containing half of the galaxies.

virialization. The observed deviation of the coefficients for R and σ from virial predictions ($\alpha = 1$, $\beta = 2$ in the formula $L \propto R_e^{\alpha}\,\sigma^{\beta}$) is interpreted as a variation of the parameters S, R_d, M/L from cluster to cluster. For example, in [33] we have shown that the mass-to-light ratio ($M_{200}/L_{K,200}$) increases with galaxy cluster mass (or luminosity). The galaxy system mass M_{200} was determined from the radial velocity dispersion, we therefore cannot use the derived mass-to-light ratio as a fourth parameter in the FP. For several galaxy systems we found independent masses $M_{X,200}$ in the literature, determined from the radiation of gas in the X-ray range. They are reported in [29], where we also give the L_K-luminosities corresponding to those masses and measured by us. For 24 galaxy groups and clusters (six systems with an underestimated, in our opinion, hydrostatic mass [29] were not part of the regression) we constructed a regression with the mass-to-light ratio:

$$\begin{aligned}\log L_K(N/2) &= 0.74(\pm0.15)\log R_e(N/2)\\ &+ 1.69(\pm0.14)\log\sigma\\ &- 0.30(\pm0.10)\log M_{X,200}/L_{K,200}\\ &+ 6.83(\pm0.07)\end{aligned}$$

and without this ratio:

$$\begin{aligned}\log L_K(N/2) &= 0.76(\pm0.18)\log R_e(N/2)\\ &+ 1.60(\pm0.16)\log\sigma + 6.19(\pm0.08).\end{aligned}$$

Fig. 8 shows the obtained dependences. We can conclude that factoring in a fourth parameter—the mass-to-K-light ratio in the FP—decreases the scatter by 12% and increases the zero-point. Apparently, in the FP for galaxy groups and clusters, the remaining scatter is due to, mainly, the degree of their deviation from the virialized state (the R_d parameter) and the

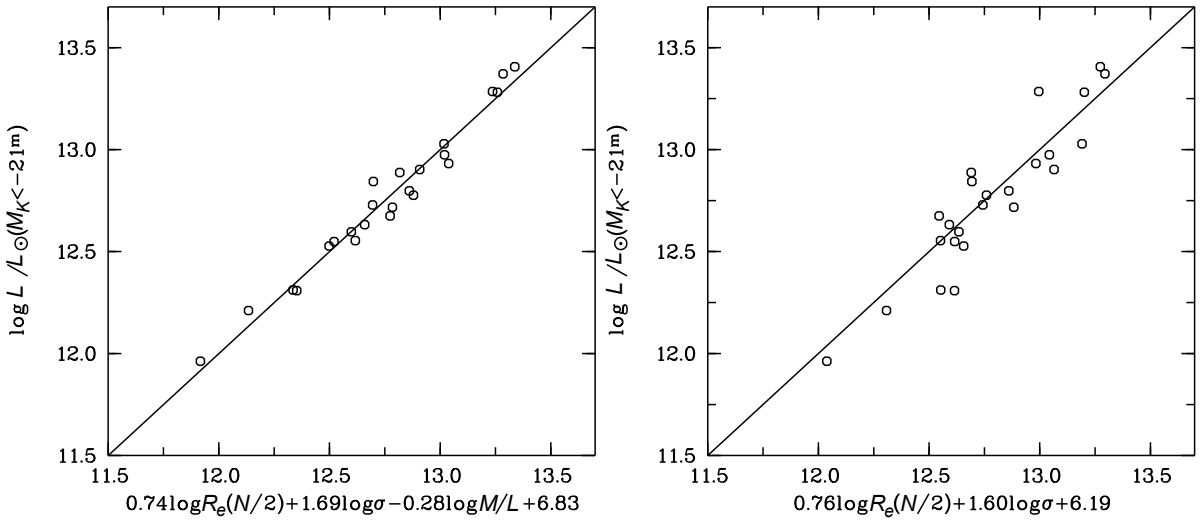

Fig. 8. Fundamental plane of 24 galaxy clusters with masses $M_{X,\,200}$ measured from gas radiation. The $M_{X,\,200}/L_{K,\,200}$ ratio is used as the fourth parameter in the FP.

corresponding system structure (the S parameter), as well as peculiar velocities. The form of the FP approaches virial predictions if the luminosity is substituted for galaxy system mass [39]. We are unable to use our mass measurements because they correlate with σ.

4. CONCLUSIONS

The scaling relations between the parameters L_K, R_e, σ, L_X, and others for galaxy groups and clusters can improve significantly our understanding of the structure of these objects and the processes of their formation and evolution. For example, in [38] it is shown that as the galaxy clusters increase, either due to absorbing individual galaxies or merging with other groups, their effective radius R_e changes. Our sample, consisting of 94 galaxy systems, has redshifts within $0.0038 < z < 0.090$; out of these systems, 50 galaxy groups have radial velocity dispersions of $\sigma < 400$ km s^{-1}, and the remaining 44 systems are galaxy clusters.

In this work, we used a simple observational method of determining the size of galaxy groups and clusters (the R_h radius) and estimating the effective radius R_e from the observed integral distribution of the number of galaxies along the squared radius from the center (Fig. 1 and Fig. 2). We determined two types of R_e radii: the radius containing half of the galaxies in the system, $(N/2)$, and the radius containing half of the system's K-luminosity $(L/2)$. As a result, we found that the luminosity of the brightest galaxy, especially in groups, can account for 50% and more of the total group luminosity contained within the effective radius R_e. Determining R_e from $L/2$ therefore gives an underestimated radius value for such groups; for 14 systems, we were unable to determine it at all using this method (the obtained radius R_e was located inside the brightest galaxy), and had to estimate R_e with prior subtraction of the luminosity of the brightest galaxy. To study all the galaxy systems in the same way, we defined their effective radius as the radius containing half of the galaxies located in the virialized region. We show that the relations between the galaxy system properties obtained this way are in agreement with the results of other authors using other methods [11, 14].

This work presents the following results for 94 galaxy groups and clusters:

1. We have constructed the fundamental plane for the stellar populations of galaxy systems in the K band:
$L_K = R_e^{0.70\pm0.13}\sigma^{1.34\pm0.13}$
or
$\log R_e = 1.03(\pm0.10)\log\sigma - 0.77(\pm0.10) + {}$
$+4.83(\pm0.11)$.

2. We have constructed fundamental planes for gas in the X-ray range:
$L_X = R_e^{1.15\pm0.39}\sigma^{2.56\pm0.40}$
and
$L_K = R_e^{0.81\pm0.21}L_X^{0.30\pm0.05}$.

3. We have found that the fundamental planes for galaxies and galaxy systems have similar shapes, but different zero-points, which is due to the fact that the mass-to-light ratio increases with luminosity (mass) of galaxy systems.

ACKNOWLEDGMENTS

This work has made use of the following databases: NASA/IPAC Extragalactic Database (NED), Sloan Digital Sky Survey (SDSS), and Two Micron All Sky Survey (2MASS).

REFERENCES

1. S. Djorgovski and M. Davis, Astrophys. J. **313**, 59 (1987).
2. A. Dressler, D. Lynden-Bell, D. Burstein, et al., Astrophys. J. **313**, 42 (1987).
3. I. Jørgensen, M. Franx, and P. Kjærgaard, Monthly Notices Royal Astron. Soc. **280**, 167 (1996).
4. M. A. Pahre, S. G. Djorgovski, and R. R. de Carvalho, Astron. J. **116**, 1591 (1998).
5. M. Bernardi, R. K. Sheth, J. Annis, et al., Astron. J. **125**, 1863 (2003).
6. A. S. Bolton, T. Treu, L. V. E. Koopmans, et al., Astrophys. J. **684**, 248 (2008).
7. R. K. Sheth and M. Bernardi, Monthly Notices Royal Astron. Soc. **422**, 1825 (2012).
8. S. M. Faber and R. E. Jackson, Astrophys. J. **204**, 668 (1976).
9. J. Kormendy, Astrophys. J. **218**, 333, (1977).
10. C. Magoulas, C. M. Springob, M. Colless, et al., Monthly Notices Royal Astron. Soc. **427**, 245 (2012).
11. M. D'Onofrio, D. Bettoni, D. Bindoni, et al., Astronomische Nachrichten **334**, 373 (2013).
12. C. Adami, A. Mazure, A. Biviano, et al., Astron. and Astrophys. **331**, 493 (1998).
13. G.J. Graves and S.M. Faber, Astrophys. J. **717**, 803 (2010).
14. R. Schaeffer, S. Maurogordato, A. Cappi, and F. Bernardeau, Monthly Notices Royal Astron. Soc. **263**, L21 (1993).
15. Y. Fujita and F. Takahara, Astrophys. J. **519**, L51 (1999).
16. C. Fritsch and T. Buchert, Astron. and Astrophys. **344**, 749 (1999).
17. M. Ramella, W. Boschin, M. Geller, et al., Astron. J. **128**, 2022 (2004).
18. K. N. Abazajian, J. K. Adelman-McCarthy, M. A. Aqüeros, et al., Astrophys. J. Suppl. **182**, 543 (2009).
19. T. H. Jarrett, T. Chester, R. Cutri, et al., Astrophys. J. **119**, 2498 (2000).
20. H. Ebeling, A. C. Edge, Böhringer, et al., Monthly Notices Royal Astron. Soc. **301**, 881 (1998).
21. A. I. Zabludoff and J. S. Mulchaey, Astrophys. J. **496**, 39 (1998).
22. A. Mahdavi and M. J. Geller, Astrophys. J. **607**, 202 (2004).
23. A. Mahdavi, M. J. Geller, H. Böhringer, et al., Astrophys. J. **518**, 69 (1999).
24. D. M. Koranyi and M. J. Geller, Astron. J. **123**, 100 (2002).
25. H. Böhringer, W. Voges, J. P. Huchra, et al., Astrophys. J. Suppl. **129**, 435 (2000).
26. M. J. Ledlow, W. Voges, F. N. Owen, and J. O. Burns, Astron. J. **126**, 2740 (2003).
27. T. H. Reiprich and H. Böhringer, Astrophys. J. **567**, 716 (2002).
28. F. G. Kopylova and A. I. Kopylov, Astrophysical Bulletin **70**, 123 (2015).
29. A. I. Kopylov and F. G. Kopylova, Astrophysical Bulletin **70**, 243 (2015).
30. R. G. Carlberg, H. K. C. Yee, E. Ellingson, et al., Astrophys. J. **485**, L13 (1997).
31. V. R. Eke, S. Cole, and C. S. Frenk, Monthly Notices Royal Astron. Soc. **282**, 263 (1996).
32. A. Biviano, ArXiv:astro-ph/0607040 (2006).
33. F. G. Kopylova and A. I. Kopylov, Astrophysical Bulletin **64**, 1 (2009).
34. K. Rines, M. J. Geller, A. Diaferio, et al., Astron. J. **128**, 1078 (2004).
35. B. Lanzoni, L. Ciotti, A. Cappi, et al., Astrophys. J. **600**, 640 (2004).
36. F. G. Kopylova and A. I. Kopylov, Astronomy Letters **40**, 659 (2014).
37. J. Kormendy and S. Dojgovski, Ann. Rev. Astron. Astrophys. **27**, 735 (1989).
38. P. A. Araya-Melo, R. van de Weygaert, and B. J. T. Jones, Monthly Notices Royal Astron. Soc. **400**, 1317 (2009).
39. N. Scott, L. M. R. Fogarty, M. S. Owers, et al., Monthly Notices Royal Astron. Soc. **451**, 2723 (2015).

Translated by E. Chmyreva